Monthly Notices
of the
ROYAL ASTRONOMICAL SOCIETY

MNRAS **479,** 4984–4990 (2018)
Advance Access publication 2018 May 3

doi:10.1093/mnras/sty1891

Testing the magnetar scenario for superluminous supernovae with circular polarimetry

Aleksandar Cikota,[1]★ Giorgos Leloudas,[2] Mattia Bulla,[3] Cosimo Inserra,[4] Ting-Wan Chen,[5]† Jason Spyromilio,[1] Ferdinando Patat,[1] Zach Cano,[6] Stefan Cikota,[7,8] Michael W. Coughlin,[9] Erkki Kankare,[10] Thomas B. Lowe,[11] Justyn R. Maund,[12] Armin Rest,[13,14] Stephen J. Smartt,[10] Ken W. Smith,[10] Richard J. Wainscoat[11] and David R. Young[10]

[1]*European Southern Observatory, Karl-Schwarzschild-Str. 2, 85748 Garching b. München, Germany*
[2]*Dark Cosmology centre, Niels Bohr Institute, University of Copenhagen, Juliane Maries vej 30, 2100 Copenhagen, Denmark*
[3]*Oskar Klein Centre, Department of Physics, Stockholm University, SE 106 91 Stockholm, Sweden*
[4]*Department of Physics & Astronomy, University of Southampton, Southampton, Hampshire, SO17 1BJ, UK*
[5]*Max-Planck-Institut für Extraterrestrische Physik, Giessenbachstraße 1, 85748, Garching, Germany*
[6]*Instituto de Astrofísica de Andalucía (IAA-CSIC), Glorieta de la Astronomía s/n, E-18008, Granada, Spain*
[7]*University of Zagreb, Faculty of Electrical Engineering and Computing, Department of Applied Physics, Unska 3, 10000 Zagreb, Croatia*
[8]*Ruđer Bošković Institute, Bijenička cesta 54, 10000 Zagreb, Croatia*
[9]*Division of Physics, Math, and Astronomy, California Institute of Technology, Pasadena, CA 91125, USA*
[10]*Astrophysics Research Centre, School of Mathematics and Physics, Queens University Belfast, Belfast BT7 1NN, UK*
[11]*Institute for Astronomy, University of Hawaii, 2680 Woodlawn Drive, Honolulu, HI 96822, USA*
[12]*Department of Physics and Astronomy, University of Sheffield, Hicks Building, Hounsfield Road, Sheffield S3 7RH, UK*
[13]*Space Telescope Science Institute, 3700 San Martin Drive, Baltimore, MD 21218, USA*
[14]*Department of Physics and Astronomy, The Johns Hopkins University, 3400 North Charles Street, Baltimore, MD 21218, USA*

Accepted 2018 April 28. Received 2018 April 27; in original form 2018 March 20

ABSTRACT

Superluminous supernovae (SLSNe) are at least ∼5 times more luminous than common supernovae. Especially hydrogen-poor SLSN-I are difficult to explain with conventional powering mechanisms. One possible scenario that might explain such luminosities is that SLSNe-I are powered by an internal engine, such as a magnetar or an accreting black hole. Strong magnetic fields or collimated jets can circularly polarize light. In this work, we measured circular polarization of two SLSNe-I with the FOcal Reducer and low dispersion Spectrograph (FORS2) mounted at the ESO's Very Large Telescope. PS17bek, a fast-evolving SLSN-I, was observed around peak, while OGLE16dmu, a slowly evolving SLSN-I, was observed 100 d after maximum. Neither SLSN shows evidence of circularly polarized light; however, these non-detections do not rule out the magnetar scenario as the powering engine for SLSNe-I. We calculate the strength of the magnetic field and the expected circular polarization as a function of distance from the magnetar, which decreases very fast. Additionally, we observed no significant linear polarization for PS17bek at four epochs, suggesting that the photosphere near peak is close to spherical symmetry.

Key words: supernovae: general – polarization – supernovae: individual: OGLE16dmu, PS17bek.

1 INTRODUCTION

Superluminous supernovae (SLSNe) may include a few remaining examples of deaths of extremely massive stars that in the early universe may have played an important role for re-ionization of the Universe and are therefore an important class of objects to understand. They are extremely bright, as the name would imply, and powering such a luminous display is a challenge. Peak luminosities of SLSNe are greater by a factor of ∼5 than peak luminosities of type Ia supernovae, and ∼10–100times greater than broad-lined type Ic and normal stripped envelope supernovae. They are sepa-

★ E-mail: acikota@eso.org
† Alexander von Humboldt Fellow

rated into two classes: the hydrogen poor SLSN-I, which have quite featureless early spectra; and hydrogen-rich SLSN-II, which are thought to occur within a thick hydrogen shell and are therefore difficult to investigate (Gal-Yam 2012).

Woosley, Blinnikov & Heger (2007) suggest that collisions between shells of matter ejected by massive stars that undergo an interior instability arising from the production of electron–positron pairs might explain such luminous SLSNe-I (see also Woosley 2016) or a pair-instability explosion of a very massive star (with a core of $\geq$50 $M_{\odot}$, e.g. Gal-Yam et al. 2009; Dessart et al. 2013). The luminosity may also be produced by interaction between the ejecta and H-poor circumstellar material (Chatzopoulos, Wheeler & Vinko 2012; Sorokina et al. 2016; Vreeswijk et al. 2017).

Another possibility is that SLSNe-I are powered by an internal engine, such as a magnetar (Kasen & Bildsten 2010; Woosley 2010; Inserra et al. 2013; Nicholl et al. 2013; Chen et al. 2015) or an accreting black hole (Dexter & Kasen 2013). Kasen & Bildsten (2010) have shown that energy deposited into an expanding supernova remnant by a highly magnetic (B $\sim 5 \times 10^{14}$G) fast-spinning neutron star can substantially contribute to the SLSN luminosity and explain the brightest events ever seen. They calculated that magnetars with initial spin periods <30 ms can reach a peak luminosity of 10^{42}–10^{45} erg s^{-1} ($M_{\rm Bol} = -16.3$ to -23.8 mag) because of the rotational energy deposition from magnetar spin-down.

In this work, we first time undertake circular polarimetry of SLSNe in the visible part of the spectrum. We aim to test the magnetar scenario using circular polarimetry. Our hypothesis is that if there is a strong magnetic field, we would expect to observe circularly polarized light, attributed to the monotonic grey-body magnetoemissivity which has been theoretically predicted by Kemp (1970) and demonstrated in the laboratory. The challenge for the magnetar observations is that the energy from the magnetar is reprocessed by the ejecta so that the bulk of the luminosity is arising from thermal processes (as is manifest in the spectra). In the thermalization process, the polarization of the original light is destroyed; however, the magnetar's magnetic field will remain.

Circular polarization has already been observed in white dwarfs with strong magnetic fields. For instance, Kemp et al. (1970) and Angel, Landstreet & Oke (1972) observed strong circular polarization, 1–3 per cent, in visible light, and 8.5–15 per cent in the infrared (Kemp & Swedlund 1970) of Grw+70°8247. For this white dwarf, they estimate a mean projected B field of 1×10^7 G.

Another possible origin of circularly polarized light may be an electron pitch-angle anisotropy in a relativistic jet, for instance from an accreting black hole, as suggested by Wiersema et al. (2014). They observed circular polarization in the afterglow of gamma-ray burst 121024A, which are believed to be powered by a collimated relativistic jet from an accreting black hole.

In Section 2, we describe the targets and observations, in Section3 the methods, in Section 4, we show the results, which we discuss in Section 5, and the summary and conclusions are presented in Section6.

2 TARGETS AND OBSERVATIONS

We obtained circular polarimetry of two SLSNe-I at single epochs: OGLE16dmu at 101.3 d past peak (rest frame), and PS17bek at peak brightness. Additionally, we obtained linear polarimetry of PS17bek at four different epochs (−4.0, +2.8, +13.4, and +21.0 d relative to peak brightness in rest frame).

All observations in this study were acquired with the FOcal Reducer and low-dispersion Spectrograph (FORS2, Appenzeller 1967; Appenzeller et al. 1998; ESO 2015) mounted at the Cassegrain focus of the UT1 Very Large Telescope (VLT), under the ESO program ID 098.D-0532(A), using the MIT CCD chip. The observations were obtained in the imaging polarimetry mode (IPOL). Circular polarimetry was obtained, without any filters, with two different quarter-wave retarder plate (QWP) angles of $\theta = \pm 45°$ but in two different rotations of the instrument (0° and 90°) in order to remove possible crosstalks between linear and circular polarization (Bagnulo et al. 2009).

Linear polarimetry of PS17bek was obtained through the V_HIGH FORS2 standard filter (λ_0= 555 nm, FWHM = 123.2 nm) at four half-wave retarder plate (HWP) angles (0°, 22.5°, 45°, and 67.5°).

A observation log is given in Table 1.

2.1 OGLE16dmu

OGLE16dmu was discovered on 2016 September 23 (MJD 57654.84) (Wyrzykowski et al. 2016) and classified as a SLSN-I. The classification spectrum is shown in Fig.1. It is apparently hostless at a redshift z $\sim$ 0.426 (Prentice et al. 2016). From GROND observations (Chen et al., in preparation), we determined an apparent magnitude at peak of m_r= 19.41 mag in 2016 November 11 (MJD 57698.41). The total Galactic reddening in the direction of OGLE16dmu is $E(B-V) = 0.03$ mag (Schlafly & Finkbeiner 2011), which corresponds to $A_r \sim 0.07$ mag assuming a Fitzpatrick (1999) extinction law and $R_V = 3.1$. The Galactic reddening-corrected absolute brightness is M_r= −22.2 mag.[1]

From the rest frame light curve, we estimate the rate of decline at 30 d past maximum (Inserra & Smartt 2014) to be $DM_{30} \sim 0.22$ mag. Alternatively, using the metric described in Nicholl et al. (2015a) (the time to reach from maximum light, $f_{\rm max}$, to $f_{\rm max}$/e), we estimate $\tau_{\rm dec} \sim$ 70.6 d. Thus, this is a bright and slowly evolving SLSN-I, similar to PTF12dam or SN 2015bn.

2.2 PS17bek

PS17bek is a SLSN-I at $z = 0.30992 \pm 0.0003$ (see Fig. 1, PESSTO classification).

It was discovered at $\alpha = 10^{\rm h}47^{\rm m}41.90^{\rm s}$ and $\delta = +26°50'06.0''$ on MJD = 57 802.4 (February 18, 2017) and it is possibly associated to the galaxy GALEXMSC J104 742.19 + 265 006.8. The object was discovered when this region of sky was observed by Pan-STARRS (Chambers et al. 2016; Smartt et al. 2016) in response to a possible low-significance gravitational wave signal provided by LIGO-Virgo (Abbott et al. 2016), but this transient was not considered related to that event. As part of the Public ESO Spectroscopic Survey for Transient Objects (PESSTO), we took a classification spectrum (see Smartt et al. 2015 for details of the instrumentation, calibration, and data access).

We determined an apparent magnitude at peak of $m_r = 19.8$ mag (Cano et al., in preparation) at MJD = 57 814.58 d. The Galactic reddening in the direction of PS17bek is $E(B-V) = 0.03$ mag (Schlafly & Finkbeiner 2011), which corresponds to $A_r \sim 0.07$ mag. Thus, the Galactic reddening-corrected absolute magnitude of PS17bek is $M_r \sim -20.7$ mag.

For PS17bek, we estimate a decline rate of $DM_{30} \sim 1.62$ mag or $t_{\rm dec} \sim 23$ d. Thus, this is a fast-declining SLSN-I, similar to SN 2010gx or SN 2011ke. In fact, the measured decline rate implies that PS17bek is one of the fastest evolving SLSNe-I (see Inserra et al.

[1]We assume a flat universe with $H_0 = 67.8$ km s^{-1} Mpc^{-1} and $\Omega_M = 0.308$ (Planck Collaboration et al. 2016).

Table 1. Observations log.

Name	UT date and time	Filter	λ/2-plate angle (°)	λ/4-plate angle (°)	Wollaston angle (°)	Exposure (s)	Seeing (')
PS17bek	2017-02-25 05:48:09	None	–	315	0	200	0.61
PS17bek	2017-02-25 05:53:59	None	–	45	0	200	0.62
PS17bek	2017-02-25 06:23:44	None	–	405	90	200	0.67
PS17bek	2017-02-25 06:28:02	None	–	135	90	200	0.61
PS17bek	2017-02-25 06:42:04	v_HIGH	0	–	0	650	0.67
PS17bek	2017-02-25 06:53:37	v_HIGH	45	–	0	650	0.63
PS17bek	2017-02-25 07:05:03	v_HIGH	22.5	–	0	650	0.66
PS17bek	2017-02-25 07:16:35	v_HIGH	67.5	–	0	650	0.55
PS17bek	2017-03-06 05:07:26	v_HIGH	0	–	0	520	0.71
PS17bek	2017-03-06 05:16:48	v_HIGH	45	–	0	700	0.60
PS17bek	2017-03-06 05:29:04	v_HIGH	22.5	–	0	700	0.59
PS17bek	2017-03-06 05:41:26	v_HIGH	67.5	–	0	700	0.50
PS17bek	2017-03-20 01:45:38	v_HIGH	0	–	0	700	0.64
PS17bek	2017-03-20 01:58:02	v_HIGH	45	–	0	700	0.69
PS17bek	2017-03-20 02:10:17	v_HIGH	22.5	–	0	700	0.70
PS17bek	2017-03-20 02:22:40	v_HIGH	67.5	–	0	700	0.86
PS17bek	2017-03-20 02:36:04	v_HIGH	0	–	0	700	0.68
PS17bek	2017-03-20 02:48:27	v_HIGH	45	–	0	700	0.67
PS17bek	2017-03-20 03:00:42	v_HIGH	22.5	–	0	700	0.77
PS17bek	2017-03-20 03:13:05	v_HIGH	67.5	–	0	700	0.81
PS17bek	2017-03-30 02:10:19	v_HIGH	0	–	0	500	0.69
PS17bek	2017-03-30 02:19:23	v_HIGH	45	–	0	500	0.72
PS17bek	2017-03-30 02:28:18	v_HIGH	22.5	–	0	500	0.68
PS17bek	2017-03-30 02:37:21	v_HIGH	67.5	–	0	500	0.56
PS17bek	2017-03-30 02:46:59	v_HIGH	0	–	0	500	0.47
PS17bek	2017-03-30 02:56:02	v_HIGH	45	–	0	500	0.54
PS17bek	2017-03-30 03:04:57	v_HIGH	22.5	–	0	500	0.58
PS17bek	2017-03-30 03:13:60	v_HIGH	67.5	–	0	500	0.81
OGLE16dmu	2017-03-30 23:59:36	None	–	315	0	220	0.74
OGLE16dmu	2017-03-31 00:04:14	None	–	45	0	220	0.85
OGLE16dmu	2017-03-31 00:18:00	None	–	405	90	220	0.84
OGLE16dmu	2017-03-31 00:22:38	None	–	135	90	220	0.75

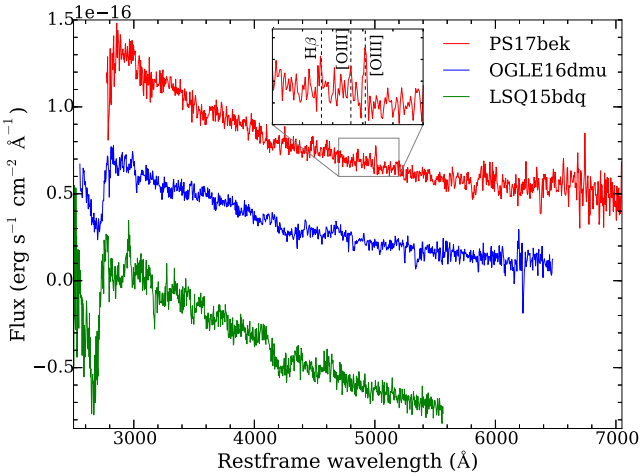

Figure 1. PESSTO classification spectra of OGLE16dmu (middle blue spectrum) and PS17bek (top red spectrum), compared to LSQ14bdq (bottom green spectrum, Nicholl et al. 2015b). The inset shows the (OIII) and Hβ emission lines in the spectrum of PS17bek, used for the redshift determination. PS17bek and LSQ14bdq have been plotted with a constant offset of $+4 \times 10^{-17}$ and -1×10^{-16}, respectively.

2018b). Starting from Gal-Yam (2012), it remains an unresolved issue if H-poor SLSNe can be divided into more sub-classes (e.g. Type I/Type R or fast/slow) and whether this division has physical implications (De Cia et al. 2017; Inserra et al. 2018b; Quimby et al. 2018). Irrespective, it remains an advantage that our experiment probes representative SLSNe from both sub-classes.

3 DATA PROCESSING AND METHODS

The data consist of two science frames per exposure: the upper CHIP1 and lower CHIP2, which correspond to two mosaic parts of the two CCD detectors. In IPOL mode, the image is split by the Wollaston prism into an ordinary (o) beam and an extraordinary (e) beam, and the multi-object spectroscopy slitlets strip mask is inserted to avoid the beams overlapping. The targets were observed at the bottom of CHIP1 (upper frame), centred in the optical axis of the telescope. The bottom strip in the upper frame is the extraordinary beam. The Wollaston prism is usually aligned with the north celestial meridian except when the instrument is rotated by 90° during the second sequence of circular polarimetry, when it was aligned towards East.

All frames were bias subtracted using the corresponding calibration bias frames. A flat-field correction was not performed because the flat-field effect gets cancelled out, because of the redundancy introduced by multiple HWP and QWP angles, for linear and circular polarimetry, respectively (Patat & Romaniello 2006; ESO 2015).

To determine the polarization of our targets, we conducted aperture photometry of sources in the ordinary and extraordinary beams using the IRAF's DAOPHOT.PHOT package. An optimal aperture radius of ∼2 FWHM was used.

3.1 Circular polarimetry

Following the FORS2 user manual (ESO 2015), the amount of circular polarization is given as:

$$V = \frac{1}{2}\left[\left(\frac{f^{o} - f^{e}}{f^{o} + f^{e}}\right)_{\theta=45^{\circ}} - \left(\frac{f^{o} - f^{e}}{f^{o} + f^{e}}\right)_{\theta=-45^{\circ}}\right], \quad (1)$$

where f^{o} and f^{e} are the measured flux in the ordinary and extraordinary beam, respectively, for both quarter-wave retarder plate angles of $\theta = \pm 45^{\circ}$. The circular polarization error was calculated by error propagation of the flux errors.

To minimize a possible linear-to-circular polarization crosstalk (Bagnulo et al. 2009), we calculate the average of the Stokes V measured at two instrument position angles, ϕ, and $\phi + 90^{\circ}$:

$$P_{V} = \frac{V_{\phi} + V_{\phi+90^{\circ}}}{2}, \quad (2)$$

which leads to cancellation of the spurious signal (Bagnulo et al. 2009).

3.2 Linear polarimetry

The Stokes Q and U parameters for PS17bek and a number of field stars were derived using the standard approach, as described in Leloudas et al. (2015), that is, via the Fourier transformation of normalized flux differences measured at four half-wave retarder plate angles of 0°, 22.5°, 45°, and 67.5° (see also the FORS2 manual, ESO 2015).

We correct the polarization position angles of the raw measurements for the half-wave plate zero angle chromatic dependence (table 4.7 of ESO 2015), and for the instrumental polarization, which increases with distance from the optical axis (fig.5 of Patat & Romaniello 2006). In addition, we used 7 field stars to determine the interstellar polarization (ISP) by calculating their barycentre in the Q–U plane for each epoch (Fig. 2). The stars give a stable and self-consistent result with time:

$Q_{\rm ISP} = 0.066 \pm 0.004$ per cent

$U_{\rm ISP} = -0.007 \pm 0.018$ per cent.

Thus, $P_{\rm ISP} = 0.066 \pm 0.004$ per cent. This value is lower than the expected maximum ISP, $p_{\rm max} = 9.0 \times E(B-V)$, determined by Serkowski, Mathewson & Ford (1975), using the Galactic reddening in the direction of PS17bek, $E(B-V) = 0.027 \pm 0.004$ mag (Schlafly & Finkbeiner 2011).

Additionally, we do a polarization bias correction, following Patat & Romaniello (2006).

4 RESULTS

We undertook circular polarimetry for two SLSNe-I: OGLE16dmu 101.3 d after peak brightness (in rest frame) and PS17bek 4.0 d before peak brightness.

The circular polarization of both SLSNe is consistent with zero. We measured a circular polarization of $P_{V} = -0.55 \pm 1.31$ per cent for OGLE16dmu, and $P_{V} = -0.21 \pm 0.18$ per cent for PS17bek. The results are summarized in Table 2. The signal-to-noise ratio of PS17bek observed at different instrument rotation angles ϕ of 0° and 90° is S/N ∼ 272 and ∼172, respectively, while for OGLE16dmu S/N ∼ 62 (at $\phi = 0^{\circ}$) and ∼59 (at $\phi = 90^{\circ}$), which explains the large uncertainties of the calculated polarization.[2]

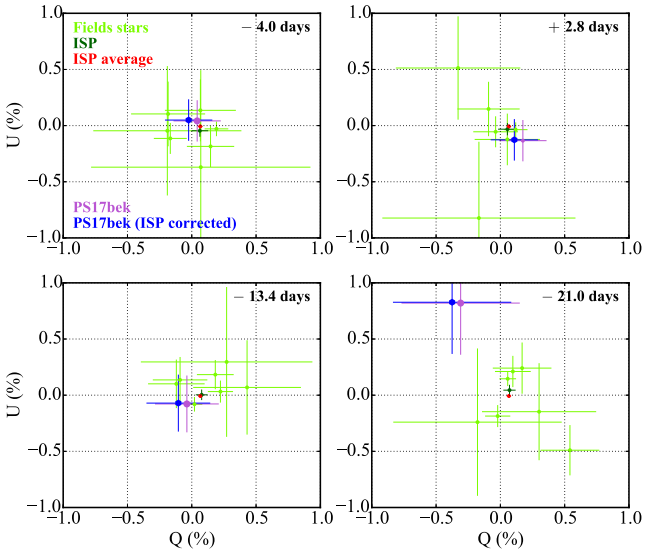

Figure 2. Q–U plane for all four epochs of PS17bek. Comparison stars are coloured light green. In each panel, a dark green cross indicates the position of the ISP, calculated as the barycentre of the stars at each epoch. The red cross is the ISP averaged over all epochs, which coincides with the dark green cross in the individual epochs. The original measurement of the SN is shown in magenta and the ISP-corrected value in blue.

Table 2. Circular polarimetry results.

SLSN	Phase	$V_{0^{\circ}}$ (%)	$V_{90^{\circ}}$ (%)	P_{V} (%)
PS17bek	−4.0 d	-0.33 ± 0.25	-0.08 ± 0.27	-0.21 ± 0.18
OGLE16dmu	+101.3 d	-0.58 ± 1.30	-0.52 ± 2.28	-0.55 ± 1.31

Fig. 3 shows a section of the FORS2 imaging polarimetry field for OGLE16dmu and PS17bek taken with different instrument position angles. It is shown that the measured polarization of our targets is consistent with the polarization of field stars that are expected to be unpolarized. Furthermore, the fainter sources with lower S/N have larger polarization values but also higher uncertainties.

The ISP-corrected linear polarization measurements of PS17bek are given in Table 3 and shown in Fig.4. At least for the first three epochs (−4, +2.8, and +13.4 relative to peak brightness), the linear polarization of the SLSN is very similar to one of the field stars and consistent with zero in Q and U. Thus, there is no significant linear polarization at these phases. The fourth epoch (21.0 d past maximum brightness) might indicate a larger polarization (∼0.8 per cent) but the result is not highly significant. The signal-to-noise ratio at the last phase is 154 (since the SN has faded), which is significantly lower than at −4 d (SNR ∼ 384), +2.8 d (SNR ∼ 384), and +13.4 d (SNR ∼ 282) relative to peak brightness. Considering that the uncertainty of the last phase is ∼0.5 per cent, this is a 2σ result.

[2]The absolute error of P is related to the signal-to-noise ratio as $\sigma_{P} = \frac{1}{\sqrt{N/2}\,SNR}$, where N is the number of wave plate angles used (Patat & Romaniello 2006).

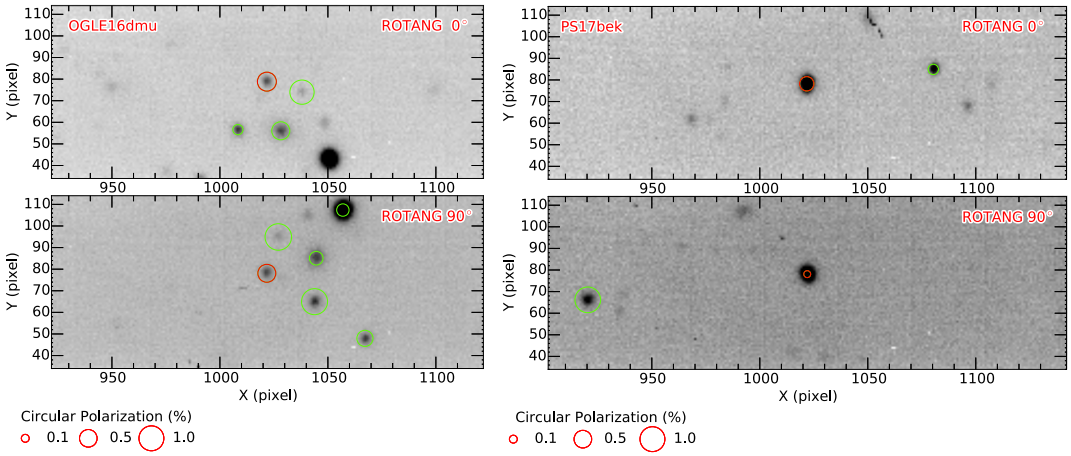

Figure 3. Sections of the ordinary beams for single imaging polarimetry exposures for OGLE16dmu (left) and PS17bek (right). The top and bottom panels are exposures taken with the instrument rotated by 0° and 90°, respectively. The red circles mark the targets, while green circles mark comparison stars in the field. The radii of the circles correspond to the absolute circular polarization, as indicated in the legend.

Table 3. ISP-corrected linear polarimetry results for PS17bek.

Phase	Q (%)	U (%)	P^a (%)	ϕ (°)
−4.0	−0.02 ± 0.18	0.05 ± 0.18	0.0 ± 0.18	56.3 ± 97.1
+2.8	0.1 ± 0.18	−0.13 ± 0.18	0.0 ± 0.18	−26.5 ± 31.6
+13.4	−0.11 ± 0.25	−0.06 ± 0.25	0.0 ± 0.25	−74.6 ± 56.8
+21.0	−0.32 ± 0.46	0.85 ± 0.46	0.19 ± 0.46	55.4 ± 14.5

Notes. [a]Polarization-bias corrected.

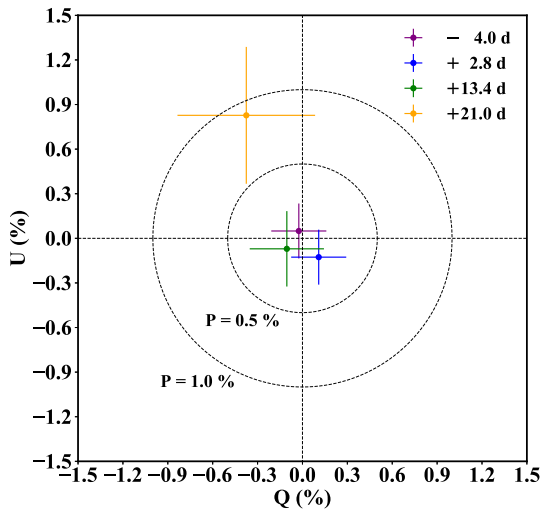

Figure 4. Stokes *Q*–*U* plane for PS17bek observed at four epochs. The different colours indicate different epochs: −4.0 (purple), +2.8 (blue), +13.4 (green), and +21.0 (yellow) days relative to peak brightness. The dashed concentric circles of equal polarization have a radius of 0.5 per cent and 1.0 per cent, respectively.

5 DISCUSSION

5.1 Circular polarimetry of OGLE16dmu and PS17bek

In the magnetar scenario, a rapidly rotating magnetar is born during a core-collapse SN explosion. The explosion ejects many solar masses of material, which expands while the magnetar spins down. The spin-down injects ∼10^{51} erg into the ejected material that has since expanded to a distance of ∼100 au, and heats it up, which then radiates the energy away (Woosley 2010; Kasen & Bildsten 2010; Inserra et al. 2013; Smith 2015).

The idea behind observing a target at early phases was to possibly detect an imprint of the strong magnetic field in the ejected material, while the aim of observing a target at late phases was to observe emitted light originating from the photosphere which moves inwards with time, closer to the magnetar, as the ejecta expands and becomes transparent.

Kemp (1970) predicted that a 'grey-body' model in a magnetic field will emit a fraction of circularly polarized light. The degree of polarization, q, is proportional to the emitting wavelength, λ, and the strength of the magnetic field, B (see equations (7) and (16) in Kemp 1970), and is given by:

$$q(\lambda) \simeq -\frac{\lambda e B}{4\pi m c}, \quad (3)$$

where e and m are the electron's charge and mass, respectively, and c is speed of light.

However, since the magnetic field is decreasing with distance, proportional to 1/distance^3, the polarization will drop very quickly. Assuming a magnetic field B_0 at the surface of a magnetar with radius R_0, the maximum magnetic field decreases as a function of distance, r, as following:

$$B(r) = B_0 \left(\frac{R_0}{r}\right)^3. \quad (4)$$

Fig. 5 shows the magnetic field, B, and the circular polarization attributed to grey-body magnetoemissivity, q, as a function of distance, calculated in the optical ($\lambda = 0.67$ μm), for three different surface magnetic strengths, B_0, for a magnetar of radius $R_0 = 10$ km.

For example, assuming a surface magnetic field strength of $B_0 = 5 \times 10^{15}$ G, the magnetic field strength drops to 4×10^4 G at a distance of only 5×10^4 km. The degree of polarization produced by grey-body magnetoemissivity at that distance is $q \sim 0.01$ per cent, which is beyond our detection capabilities.

Furthermore, our observations were taken without any filter in order to achieve a high SNR in a reasonable time, while the absolute degree of circular polarization produced by grey-body magnetoemissivity increases with wavelength (see equation 3). Therefore, it is

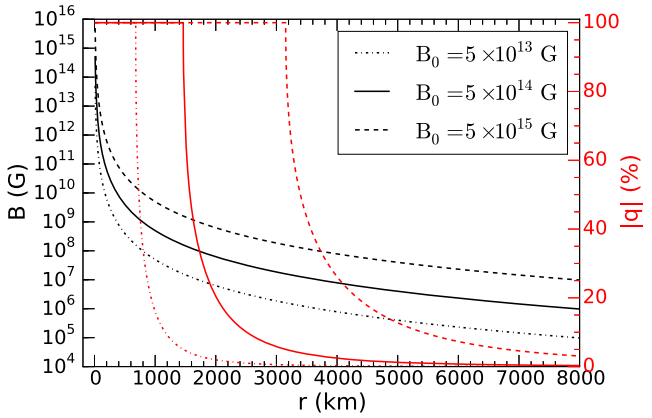

Figure 5. Maximum magnetic field strength (black lines) and absolute circular polarization, q (red lines), in the optical ($\lambda = 0.67\ \mu$m) as a function of distance, r, for three different initial surface magnetic field strengths, B_0, at $R_0 = 10$ km.

generally recommended to observe circular polarization at infrared wavelengths.

Despite a non-detection of circular polarization in SLSN-I, the magnetar scenario cannot be excluded as the internal engine of SLSNe, because in order to observe circularly polarized light attributed to grey-body magnetoemissivity, it is necessary that the light is emitted within strong magnetic fields, close to the magnetar, which is not the case in the magnetar scenario as described, e.g. by Kasen & Bildsten (2010), in contrast to the observed circular polarization in white dwarfs (e.g. Kemp, Swedlund & Wolstencroft 1971; Rich & Williams 1973), where the observed light is emitted from the white dwarf's surface.

Another possibility for the lack of observed circular polarization is that OGLE16dmu and PS17bek are not driven by an internal engine at all. For instance, other possible scenario that could explain such a high luminosity is a pair-instability supernova (PISN, e.g. Woosley et al. 2007; Gal-Yam et al. 2009; Dessart et al. 2013; Woosley 2016; Kozyreva 2017), or a normal SN explosion interacting with circumstellar shells (e.g. Chatzopoulos et al. 2012; Sorokina et al. 2016; Vreeswijk et al. 2017). In case of a PISN, which requires high amounts of ^{56}Ni to explain the luminosity, the light curves are expected to evolve slowly, which likely rules out this scenario for PS17bek that has one of the fastest evolving light curves (Chen et al., in preparation). However, it is beyond the scope of this short paper to analyse the light curves for those SLSNe.

5.2 Linear polarimetry of PS17bek

Intrinsic linear polarization of SNe is a measure of the supernova's photosphere departure from spherical symmetry projected on the sky. If the projection of the photosphere is not symmetric, more photons will be scattered by electrons along the photosphere's major axis than along the minor axis, which will produce net polarization in the continuum (see, e.g. Hoflich 1991; Kasen et al. 2003; Bulla, Sim & Kromer 2015).

Because SLSNe are faint, and thus it is hard to undertake polarimetry that requires high SNR, only a few SLSNe have been studied using polarimetry (Leloudas et al. 2015; Inserra et al. 2016, 2018a; Leloudas et al. 2017; Bose et al. 2018).

LSQ14mo, also a fast-declining SLSN-I (as PS17bek), did not show evidence for significant polarization or polarization evolution from −7 and up to +19 d with respect to maximum (Leloudas et al. 2015). In the contrary, the slowly evolving SN 2015bn did show an increase in polarization with time that was attributed to the photosphere receding to inner layers of the explosion that are more asymmetric. Inserra et al. (2016) obtained the first spectropolarimetric observations of an SLSN-I, at −24 and +28 d, further showing that the geometry was consistent with an axisymmetric configuration (that could be consistent with a magnetar scenario). The polarization increase was confirmed by Leloudas et al. (2017), who obtained multi-epoch imaging polarimetry between −20 and +46 d, showing that the increase was coincident with changes in the optical spectrum.

The result obtained for PS17bek is fairly consistent with the picture obtained from previous events. Similar to the other SLSNe-I, observed around peak, no significant polarization is detected. Our last observation (at +21 d) could be consistent with an increase in polarization but the significance of this result is below 2σ. Either fast-evolving SLSNe (PS17bek and LSQ14mo) follow a different geometrical evolution than slowly evolving SLSNe, or simply the available data, due to a combination of low SNR and lack of data at late phases, are not able to significantly detect an increase in polarization.

6 SUMMARY AND CONCLUSIONS

In this work, we investigated circular polarization of two hydrogen-poor SLSNe for the first time, using FORS2 at the VLT. Our main results can be summarized as follows:

(i) OGLE16dmu is a slowly evolving hydrogen-poor SLSN. We undertook circular imaging polarimetry at +101.3 d past peak (in rest frame r band) and found no evidence of circular polarization.

(ii) PS17bek is a fast-evolving SLSN-I. We undertook circular polarimetry at −4.0 d relative to the peak brightness (in rest frame r band) and found no evidence of circular polarization.

(iii) Additionally, PS17bek was observed in linear polarimetry mode at four phases (−4.0, +2.8, +13.4, and +21.0 d), and shows no significant linear polarization.

(iv) We cannot exclude the magnetar scenario because of a non-detection of circular polarization, which, due to the rapid decrease in the strength of the magnetic with distance, would be detectable only at small radii close to the surface of the magnetar.

(v) We note that future attempts to measure the strength of magnetic fields using circular polarimetry should be made in the infrared, where the expected degree of circular polarization produced by grey-body magnetoemissivity is higher.

(vi) It is not likely that we will observe circular polarization produced by grey-body magnetoemissivity, because (assuming the magnetar scenario) the bulk of the luminosity arises from thermal processes in the ejecta, which occurs at large distances from the magnetar, where the magnetic fields are not strong enough to produce significant circular polarization, however, such observations are valuable, because they may also allow us to probe for other sources of circular polarization, e.g relativistic jets.

ACKNOWLEDGEMENTS

We thank Daniele Malesani for useful discussion. This work is on observations made with ESO Telescopes at the Paranal Observatory under the programme ID 098.D-0532(A) and PESSTO (Public ESO Spectroscopic Survey for Transient Objects), ESO programme ID 197.D-1075. SJS acknowledges STFC funding through grant ST/P000312/1. MB acknowledges support from the Swedish Re-

search Council (Vetenskapsrådet) and the Swedish National Space Board. TWC acknowledges the funding provided by the Alexander von Humboldt Foundation. This research was supported by the Munich Institute for Astro- and Particle Physics (MIAPP) of the DFG cluster of excellence "Origin and Structure of the Universe".

REFERENCES

Abbott B. P. et al., 2016, ApJ, 826, L13
Angel J. R. P., Landstreet J. D., Oke J. B., 1972, ApJ, 171, L11
Appenzeller I., 1967, PASP, 79, 136
Appenzeller I. et al., 1998, The Messenger, 94, 1
Bagnulo S., Landolfi M., Landstreet J. D., Landi Degl'Innocenti E., Fossati L., Sterzik M., 2009, PASP, 121, 993
Bose S. et al., 2018, ApJ, 853, 57
Bulla M., Sim S. A., Kromer M., 2015, MNRAS, 450, 967
Chambers K. C. et al., 2016, preprint (arXiv:1612.05560)
Chatzopoulos E., Wheeler J. C., Vinko J., 2012, ApJ, 746, 121
Chen T.-W. et al., 2015, MNRAS, 452, 1567
De Cia A. et al., 2017, preprint (arXiv:1708.01623)
Dessart L., Waldman R., Livne E., Hillier D. J., Blondin S., 2013, MNRAS, 428, 3227
Dexter J., Kasen D., 2013, ApJ, 772, 30
ESO 2015, FORS2 User Manual, issue 96.0, VLT-MAN-ESO-13100-1543. European Southern Observatory, Garching bei München, Germany
Fitzpatrick E. L., 1999, PASP, 111, 63
Gal-Yam A., 2012, Science, 337, 927
Gal-Yam A. et al., 2009, Nature, 462, 624
Hoflich P., 1991, A&A, 246, 481
Inserra C., Bulla M., Sim S. A., Smartt S. J., 2016, ApJ, 831, 79
Inserra C., Prajs S., Gutierrez C. P., Angus C., Smith M., Sullivan M., 2018b, ApJ, 854, 175
Inserra C., Smartt S. J., 2014, ApJ, 796, 87
Inserra C. et al., 2013, ApJ, 770, 128
Inserra C. et al., 2018a, MNRAS, 475, 1046
Kasen D., Bildsten L., 2010, ApJ, 717, 245
Kasen D., et al., 2003, Apj, 593:788
Kemp J. C., 1970, ApJ, 162, 169
Kemp J. C., Swedlund J. B., 1970, ApJ, 162, L67
Kemp J. C., Swedlund J. B., Landstreet J. D., Angel J. R. P., 1970, ApJ, 161, L77
Kemp J. C., Swedlund J. B., Wolstencroft R. D., 1971, ApJ, 164, L17
Kozyreva A., Gilmer M., Hirschi R. et al., 2017, MNRAS, 464, 2854
Leloudas G. et al., 2015, ApJ, 815, L10
Leloudas G. et al., 2017, ApJ , 837, L14
Nicholl M. et al., 2013, Nature, 502, 346
Nicholl M. et al., 2015a, MNRAS, 452, 3869
Nicholl M. et al., 2015b, ApJ, 807, L18
Patat F., Romaniello M., 2006, PASP, 118, 146
Planck Collaboration et al., 2016, A&A, 594, A13
Prentice S. et al., 2016, The Astronomer's Telegram, 9542
Quimby R. M. et al., 2018, ApJ, 855, 2
Rich A., Williams W. L., 1973, ApJ, 180, L123
Schlafly E. F., Finkbeiner D. P., 2011, ApJ, 737, 103
Serkowski K., Mathewson D. S., Ford V. L., 1975, ApJ, 196, 261
Smartt S. J. et al., 2015, A&A, 579, A40
Smartt S. J. et al., 2016, MNRAS, 462, 4094
Smith N., 2015, Observed Consequences of Preupernova Instability in Very Massive Stars. Springer International Publishing, Cham , Switzerland, p. 227
Sorokina E., Blinnikov S., Nomoto K., Quimby R., Tolstov A., 2016, ApJ, 829, 17
Vreeswijk P. M. et al., 2017, ApJ, 835, 58
Wiersema K. et al., 2014, Nature, 509, 201
Woosley S. E., 2010, ApJ, 719, L204
Woosley S. E., 2017, ApJ, 836, 24
Woosley S. E., Blinnikov S., Heger A., 2007, Nature, 450, 390
Wyrzykowski L. et al., 2016, Astron. Telegram, 954

This paper has been typeset from a TEX/LATEX file prepared by the author.